33. X. Vernede, J. C. Fontecilla-Camps, *J. Appl. Crystallogr.* **32**, 505 (1999).
34. Collaborative computational project, *Acta Crystallogr.* **D50**, 760 (1994).
35. A. T. Brünger, *X-PLOR version 3.1: A System for X-ray Crystallography and NMR* (Yale Univ. Press, New Haven, CT, 1992).
36. A. T. Brünger *et al.*, *Acta Crystallogr.* **D54**, 905 (1998).
37. D. Kern *et al.*, *Science* **275**, 67 (1997).
38. A. Roussel, C. Cambillaud, *Turbo-Frodo* (Silicon Graphics, Mountain View, CA, 1989), p. 77.
39. P. J. Kraulis, *J. Appl. Crystallogr.* **24**, 946 (1991).
40. E. A. Merritt, D. J. Bacon, *Methods Enzymol.* **277**, 505 (1997).
41. We thank the staff of beamline ID-14 of the European Synchrotron Radiation Facility for help during data collection and S. Ragsdale, M. Fontecave, P. Amara, M. Field, and E. Mulliez for critical reading of the manuscript. E.C. was the recipient of a fellowship from the French Ministry of Research. This work was supported by the Commisariat à l'Energie Atomique and the CNRS. Coordinates and structure factors have been deposited in the Protein Data Bank, with accession code 1kek.

12 September 2001; accepted 2 November 2001

KLF6, a Candidate Tumor Suppressor Gene Mutated in Prostate Cancer

Goutham Narla,[1] Karen E. Heath,[2]* Helen L. Reeves,[1]* Dan Li,[1] Luciana E. Giono,[1] Alec C. Kimmelman,[3] Marc J. Glucksman,[4]† Jyothsna Narla,[7] Francis J. Eng,[1] Andrew M. Chan,[3] Anna C. Ferrari,[3,5] John A. Martignetti,[2,3,6] Scott L. Friedman[1]‡

Kruppel-like factor 6 (*KLF6*) is a zinc finger transcription factor of unknown function. Here, we show that the *KLF6* gene is mutated in a subset of human prostate cancer. Loss-of-heterozygosity analysis revealed that one *KLF6* allele is deleted in 77% (17 of 22) of primary prostate tumors. Sequence analysis of the retained *KLF6* allele revealed mutations in 71% of these tumors. Functional studies confirm that whereas wild-type KLF6 up-regulates p21 (WAF1/CIP1) in a p53-independent manner and significantly reduces cell proliferation, tumor-derived KLF6 mutants do not. Our data suggest that *KLF6* is a tumor suppressor gene involved in human prostate cancer.

Prostate cancer is a leading cause of cancer death in men, with more than 198,000 new cases and 32,000 deaths annually in the United States alone. Loss of heterozygosity (LOH) analyses of sporadic prostate cancers and linkage studies of familial prostate cancer have provided strong evidence for the existence of prostate cancer–susceptibility genes (*1*). Although a number of tumor suppressor genes, including the retinoblastoma susceptibility gene (*RB1*), the putative protein tyrosine phosphatase gene (*PTEN*), and *p53*, have been implicated in prostate cancer, no single gene has yet been identified which is responsible for the majority of cases (*2*).

KLF6 (*Zf9/CPBP*) (GenBank accession number AF001461) is a ubiquitously expressed Kruppel-like transcription factor whose in vivo role has not been fully clarified (*3–5*). *KLF6* contains a proline- and serine-rich NH_2-terminal activation domain, and like other Kruppel-like factors, three COOH-terminal C2H2 zinc fingers. *KLF6* directly interacts with DNA through a GC box promoter element (*3*). Putative transcriptional targets of *KLF6* include the genes encoding a placental glycoprotein (*4*), collagen α1(I) (*3*), transforming growth factor β1 (*TGFβ1*), types I and II *TGFβ* receptors (*6*), urokinase type plasminogen activator (*uPA*) (*7*), and the human immunodeficiency virus long terminal repeat (*HIV-1 LTR*) (*5*).

The *KLF6* gene maps to human chromosome 10p, a region deleted in ~55% of sporadic prostate adenocarcinomas (*8, 9*). Given the role of Kruppel-like factors in the regulation of many cellular processes that include differentiation and development (*10*), we examined primary prostate tumor samples for specific LOH of the *KLF6* gene. Microsatellite markers flanking *KLF6* were analyzed in paired normal prostate tissue and in well to poorly differentiated prostate tumor specimens from 22 patients (*11, 12*). Of the 22 samples analyzed, 17 (77%) displayed LOH of the *KLF6* locus (Fig. 1A). To define the minimal region of loss, we designed two microsatellite markers, *KLF6M1* and *KLF6M2*, which flank the *KLF6* gene by ~42 kb and ~12 kb, respectively (*12*). Tumor DNA from patients 9 and 10 showed loss of only the tightly flanking *KLF6M1* and *KLF6M2* microsatellite markers, whereas that from patients 14 and 21 demonstrated loss of only *KLF6M1* (Fig. 1A). Representative fluorescent electropherograms for microdissected tumor samples with loss of *KLF6M1* are shown in Fig. 1B.

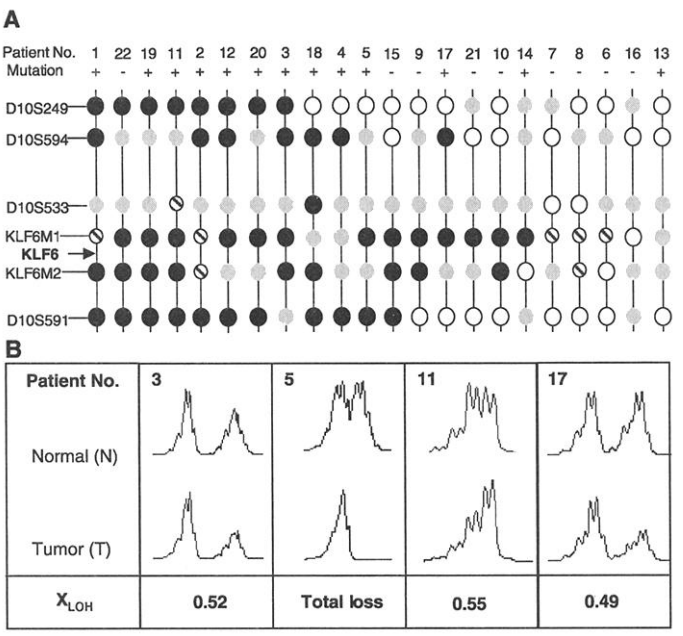

Fig. 1. LOH at the *KLF6* locus in human prostate tumors. **(A)** Summary of LOH patterns of 22 prostate tumors. Retained microsatellite markers are indicated in white, markers demonstrating allelic loss in black, and noninformative markers in gray. A hatched circle indicates DNA that could not be amplified. Patient data was grouped according to degree of LOH. Genetic map is not drawn to scale. **(B)** Representative fluorescent electropherograms for microsatellite marker *KLF6*M1 for patients with LOH. A X_{LOH} score of less than 0.7 was used for determination of LOH (*12*).

[1]Division of Liver Diseases, Department of Medicine, [2]Department of Human Genetics, [3]The Derald H. Ruttenberg Cancer Center, [4]Department of Neurobiology, [5]Division of Medical Oncology, Department of Medicine, and [6]Department of Pediatrics, Mount Sinai School of Medicine, 1425 Madison Avenue, Room 1170F, Box 1123, New York, NY, 10029, USA. [7]Regional Medical Center, 225 North Jackson, San Jose, CA, 95116, USA.

*These authors contributed equally to this work.
†Present address: Structural Neurobiology and Proteomics Laboratory, Department of Biochemistry and Molecular Biology, FUHS/Chicago Medical School, 3333 Green Bay Road, North Chicago, IL 60064, USA.
‡To whom correspondence should be addressed. E-mail: frieds02@doc.mssm.edu

We then sequenced all four coding exons and intron-exon boundaries of the retained *KLF6* allele using genomic DNA from these 22 tumors (*13*). Twelve of 17 (71%) tumor samples showing LOH of *KLF6* had mutations in the retained *KLF6* allele (Fig. 1A and Fig. 2, A and B), suggesting that two inactivating events had occurred; thus, as defined by Knudson's "two-hit model" (*14*), *KLF6* appears to be a tumor suppressor gene. No mutations were present in the paired normal prostate tissue genomic DNA from these patients, confirming that the tumor-derived mutations were somatic. Analysis of 11 additional prostate cancer patients for which there was insufficient normal DNA available to complete LOH studies also revealed *KLF6* mutations in five of the tumors (*12*).

Interestingly, a number of tumor samples showed compound mutations in *KLF6* (Fig. 2B). The presence of multiple single-gene mutations within the same tumor is unusual, but genetic heterogeneity in prostate cancer has been reported previously for the tumor suppressor *p53* (*15, 16*). Here, we show that separate malignant foci within the same tumor can harbor distinct *KLF6* mutations. We used laser capture microdissection (LCM) to isolate malignant tissue (2,500 to 10,000 cells) from separate tumor foci (*12*) within the same tumor in six patients. Five of these patients had *KLF6* mutations. In three, the mutation was seen in DNA derived from the cells of one tumor focus and not the other. Furthermore, two patients had distinct *KLF6* mutations in different tumor foci. No mutations were detected in the adjacent normal prostate tissue.

In total, 18 of 33 prostate tumors (55%) had *KLF6* mutations. Of the 26 mutations identified, 23 were within the *KLF6* transactivation domain (*12*). These mutations resulted in 25 nonconservative amino acid changes and the introduction of a premature stop codon. None of these mutations was present in the patient's normal prostate tissue DNA or in germline DNA from 100 chromosomes of 50 unaffected, unrelated individuals. The majority of the mutations affected highly conserved amino acids, suggesting that these residues are functionally important.

To explore the biological activity of *KLF6*, we generated an NIH 3T3 cell line in which *KLF6* expression was regulated by a tetracycline (tet)-responsive promoter (*12*). Up-regulation of wild-type (wt) *KLF6* significantly ($P < 0.001$) reduced cell proliferation (Fig. 3A). Induction of KLF6 resulted in a fivefold increase in the expression of p21 (WAF1/CIP1), an inhibitor of several cyclin-dependent kinases and a key regulator of the G_1/S transition (*17*), and a reduction in proliferating cell nuclear antigen (PCNA) expression (Fig. 3B) (*12*). Transient cotransfection assays with wt KLF6 and a *p21* promoter luciferase reporter construct revealed that *p21* is a direct transcriptional target of *KLF6* (Fig. 3C) (*12*). Transient cotransfection performed with wt KLF6 and *p21* promoter deletion constructs (*18*) revealed that upstream flanking sequences including two GC boxes present in only the deletion construct pW-*225* were necessary for high-level transactivation of the *p21* promoter by KLF6 (Fig. 3D). Gel shift using oligonucleotides corresponding to these wt and mutated "GC box" motifs further indicated that transactivation of the *p21* promoter by *KLF6* is mediated through binding to these two GC boxes (*12*). Additional studies have confirmed that *KLF6* up-regulates *p21* and suppresses growth in a p53-independent manner (*12*).

To determine the effect of tumor-derived mutations on *KLF6* function in this cell culture assay system, we generated cDNAs encoding four KLF6 protein mutants (*12*) and performed transient cotransfection assays with a *p21* promoter reporter (Fig. 4A). Wild-

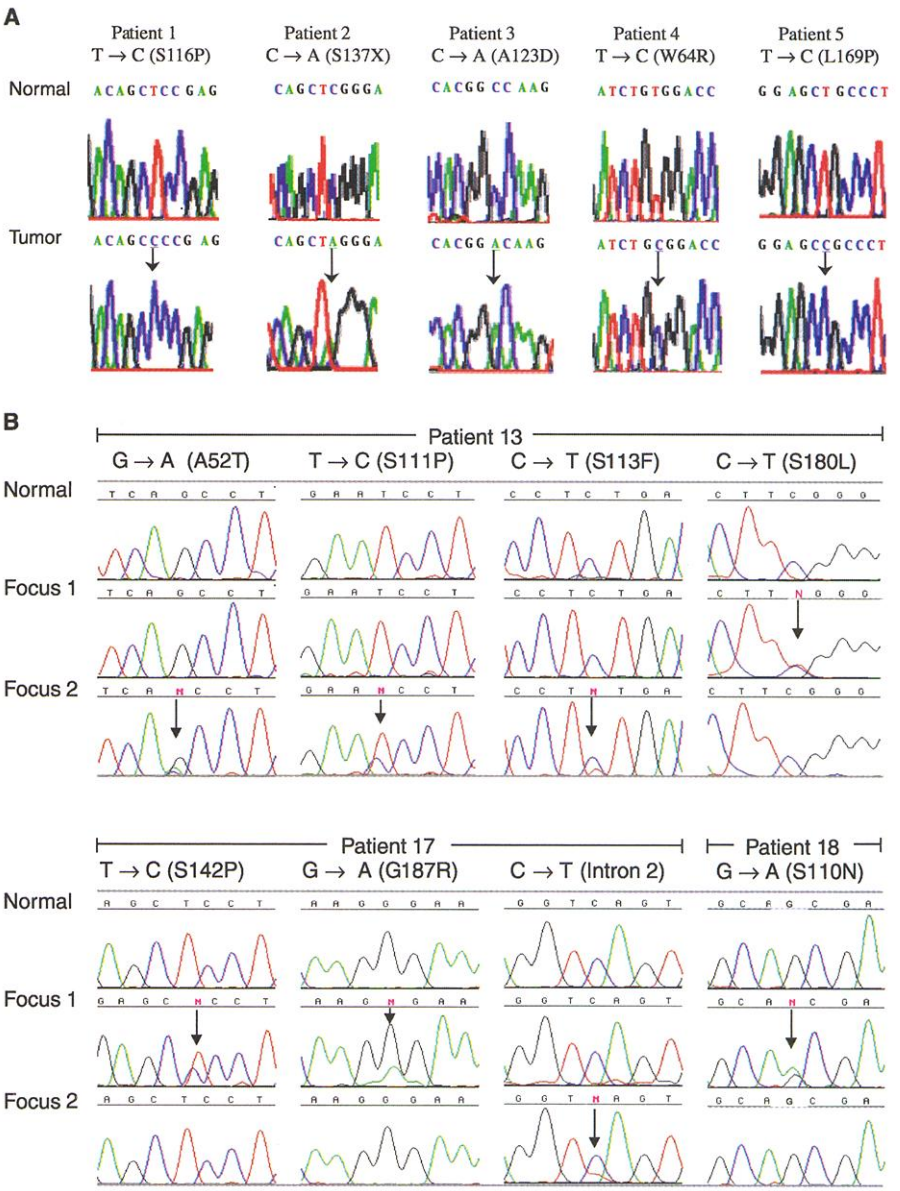

Fig. 2. Sequence analysis reveals *KLF6* mutations in human prostate tumors. **(A)** Tumor samples from patients 1 through 5 showed LOH of the *KLF6* locus. Sequence analysis of *KLF6* was performed on PCR-amplified and subcloned tumor-derived genomic DNA, which was then used in functional studies. The mutations are underlined. **(B)** LCM was used to isolate normal and malignant cells from distinct foci within the same tumor. DNA sequence analysis was performed using genomic DNA extracted from each malignant focus and from surrounding normal prostate tissue. Separate malignant foci (Focus 1 and Focus 2) from the same patient contained different *KLF6* mutations (Patient 13 and Patient 17). Patient 18 had a *KLF6* mutation in Focus 1 but not in Focus 2. Mutations are indicated by an "N" in the sequencing chromatogram. No mutations were detected in the adjacent normal prostate tissue, confirming that the mutations were somatic.

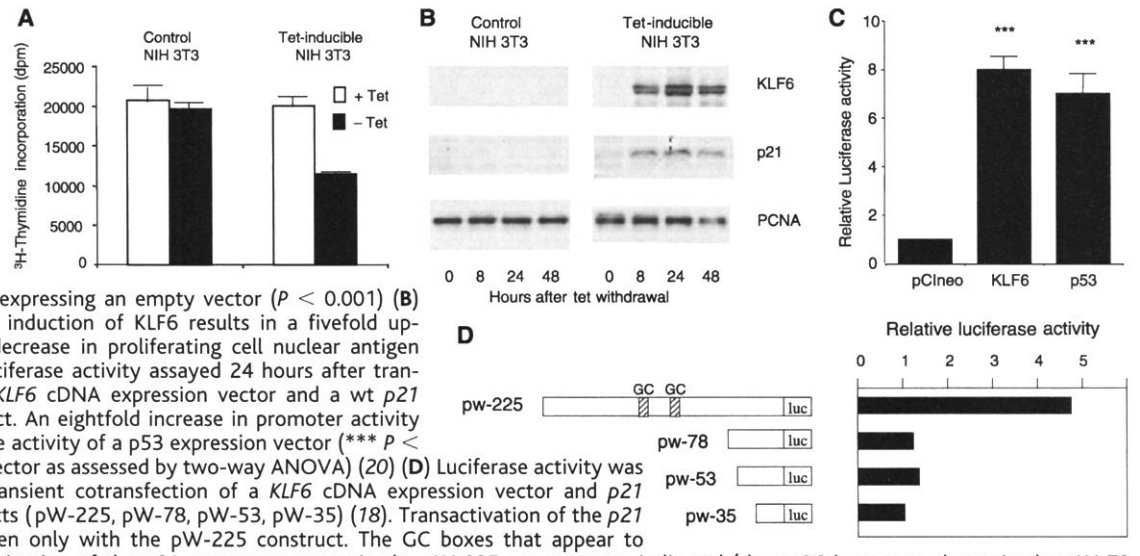

Fig. 3. *p21 (WAF1/CIP1)* is a direct transcriptional target of *KLF6*. **(A)** DNA synthesis was assayed in NIH 3T3 fibroblasts expressing KLF6 under the regulation of a tetracycline (tet) responsive promoter. Induction of KLF6 by 24-hour withdrawal of tet reduced cell proliferation by 40% compared to control cells expressing an empty vector ($P < 0.001$) **(B)** Immunoblot showing that induction of KLF6 results in a fivefold up-regulation of p21 and a decrease in proliferating cell nuclear antigen (PCNA) expression. **(C)** Luciferase activity assayed 24 hours after transient cotransfection of a *KLF6* cDNA expression vector and a wt *p21* promoter reporter construct. An eightfold increase in promoter activity was detected, similar to the activity of a p53 expression vector (*** $P < 0.0001$ relative to empty vector as assessed by two-way ANOVA) (*20*) **(D)** Luciferase activity was assayed 24 hours after transient cotransfection of a *KLF6* cDNA expression vector and *p21* promoter deletion constructs (pW-225, pW-78, pW-53, pW-35) (*18*). Transactivation of the *p21* promoter by KLF6 was seen only with the pW-225 construct. The GC boxes that appear to mediate high-level transactivation of the *p21* promoter present in the pW-225 construct are indicated (these GC boxes are absent in the pW-78, pW-53, and pW-35 constructs).

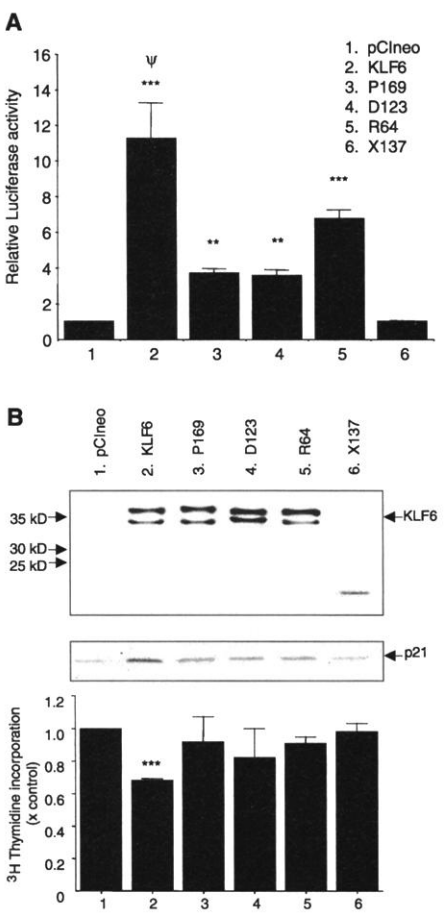

Fig. 4. Prostate cancer-derived *KLF6* mutants show loss of growth suppressive activity. **(A)** Luciferase activity was assayed 24 hours after cotransfection of an immortalized human embryonal fibroblast cell line (293T) with a *p21* promoter reporter construct containing mutated p53 binding sites and the indicated mutant or wt KLF6. A 10-fold increase in *p21*- promoter activity was detected following expression of wt KLF6 (*** $P < 0.0001$). The X137 truncation mutant had no transactivating activity and the remaining three tumor-derived mutants transactivated the *p21* promoter (** $P < 0.05$) to a lesser extent than wt KLF6 (ψ indicates a $P < 0.0001$ relative to KLF6 mutants by two-way ANOVA) (*20*). **(B)** PC3 cells were transfected with the R64, D123, X137, P169 tumor-derived mutant proteins or wt human KLF6. Cells were harvested 24 hours later and KLF6 and p21 expression levels were determined by Western blot. All four mutant proteins were expressed. Numbers on the left indicate size in kilodaltons. A threefold up-regulation of endogenous p21 was detected with the wt KLF6 determined by band densitometry ($n = 4$, $P < 0.001$ relative to empty vector). In contrast, there was no significant up-regulation of p21 by any of the tumor-derived mutants. DNA synthesis was assayed 40 hours after PC3 cells were transfected with wt or mutant KLF6 protein. DNA synthesis in cells transfected with wt KLF6 was suppressed by 40% compared to empty vector transfected cells (*** $P < 0.0001$, $n = 6$, two-way ANOVA) (*20*). None of the tumor-derived mutants significantly suppressed DNA synthesis ($n = 4$).

type KLF6 transactivated the *p21* promoter 10-fold, whereas none of the four tumor-derived mutants were active to a similar level ($P < 0.0001$). Unlike wt KLF6, none of these mutants significantly up-regulated the endogenous level of p21 (Fig. 4B) or significantly suppressed the growth of prostate cancer 3 (PC3) cells (Fig. 4B).

Of the four missense mutations in the DNA binding domain (amino acids 201 to 283) (*3, 12*), two are predicted to disrupt the critical zinc finger motifs in the protein and thus could conceivably alter protein function. The $Cys^{265} \rightarrow Tyr^{265}$ (C265Y) mutation, which occurs in the last zinc finger, is predicted to prevent zinc binding (*19*) and hence might affect *KLF6*-DNA interactions. The $Leu^{217} \rightarrow Ser^{217}$ (L217S) mutation affects a residue conserved across 20 zinc finger–containing domains, and this leucine aligns perfectly with the initial cysteine of the three zinc fingers and would therefore be predicted to affect secondary structure. In addition, examination of the primary sequence revealed mutations involving known phosphorylation motifs.

Our data identify *KLF6* as a candidate tumor suppressor gene in prostate cancer. Given its ubiquitous expression and its ability to suppress growth, *KLF6* may have a general role in the development or progression of other human cancers, particularly those associated with LOH at chromosome 10p15.

References and Notes

1. E. A. Ostrander, J. L. Stanford, *Am. J. Hum. Genet.* **67**, 1367 (2000).
2. A. Latil, R. Lidereau, *Virchows Arch.* **432**, 389 (1998).
3. V. Ratziu *et al.*, *Proc. Natl. Acad. Sci. U.S.A.* **95**, 9500 (1998).
4. N. P. Koritschoner *et al.*, *J. Biol. Chem.* **272**, 9573 (1997).
5. T. Suzuki *et al.*, *J. Biochem.* **124**, 389 (1998).
6. Y. Kim *et al.*, *J. Biol. Chem.* **273**, 33750 (1998).
7. S. Kojima *et al.*, *Blood* **95**, 1309 (2000).
8. M. Ittmann, *Cancer Res.* **56**, 2143 (1996).
9. T. M. Trybus, A. C. Burgess, K. J. Wojno, T. W. Glover, J. A. Macoska, *Cancer Res.* **56**, 2263 (1996).
10. J. J. Bieker, *J. Biol. Chem.* **276**, 34355 (2001).
11. Microsatellite analysis was performed using fluorescently labeled microsatellite markers flanking *KLF6* and ordered according to the Marshfield map. A relative allele ratio, X_{LOH}, of less than 0.7 was defined as loss of heterozygosity (*12*).
12. Supplementary material is available on *Science* Online at www.sciencemag.org/cgi/content/full/294/5551/2563/DC1
13. Mutations in patients 1 through 5 were from matched normal and tumor-derived genomic DNA subcloned into an expression vector, which were then used in functional studies. All other mutations were detected by direct sequencing of polymerase chain reaction (PCR) products. All results were confirmed by sequencing in both directions (*12*).

14. A. G. Knudson, *Proc. Natl. Acad. Sci. U.S.A.* **68**, 820 (1971).
15. D. Mirchandani *et al.*, *Am. J. Pathol.* **147**, 92 (1995).
16. P. H. Gumerlock *et al.*, *J. Natl. Cancer. Inst.* **89**, 66 (1997).
17. C. J. Sherr, J. M. Roberts, *Genes Dev.* **13**, 1501 (1999).
18. D. M. Prowse, L. Bolgan, A. Molnar, G. P. Dotto, *J. Biol. Chem.* **272**, 1308 (1997).
19. C. A. Kim, J. M. Berg, *Nature Struct. Biol.* **3**, 940 (1996).
20. Results are expressed as mean ± standard error. Statistical analysis was performed using a two-way analysis of variance (ANOVA). For direct comparisons between groups, the Bonferonni correction has been applied.
21. We thank J. Friedman, M. Oren, N. Mohandas, and Z. Ronai for helpful advice and P. Dotto, B. Li, M. Mari, D. Musat, T. Ouchi, M. Ramirez, and P. Unger for technical assistance. Supported by grants from the NIH (DK37340 to S.L.F, CA79918 to A.C.F., and CA78207 to A.C.K.), Mount Sinai School of Medicine Dean's Research Incentive Fund (S.L.F.) and Child Health Research Center (5 P30 HD28822 to J.A.M.), Charles H. Revson Foundation (K.E.H.), Howard Hughes Medical Institute (G.N.), American Liver Foundation (G.N.), University of Newcastle upon Tyne Department of Medicine (H.L.R.), and the Peel Medical Research Trust, UK (H.L.R.).

18 September 2001; accepted 6 November 2001

Independent and Redundant Information in Nearby Cortical Neurons

Daniel S. Reich,[1,2]* Ferenc Mechler,[2] Jonathan D. Victor[2]

In the primary visual cortex (V1), nearby neurons are tuned to similar stimulus features, and, depending on the manner and time scale over which neuronal signals are analyzed, the resulting redundancy may mitigate deleterious effects of response variability. We estimated information rates in the short–time scale responses of clusters of up to six simultaneously recorded nearby neurons in monkey V1. Responses were almost independent if we kept track of which neuron fired each spike but were redundant if we summed responses over the cluster. Redundancy was independent of cluster size. Summing neuronal responses to reduce variability discards potentially useful information, and the discarded information increases with cluster size.

How do neurons in the sensory cortex work together to represent a stimulus? Cortical neurons with similar stimulus selectivities are found in close proximity to one another (*1–3*). This might reflect a mechanism of coping with large trial-to-trial variability in the responses of individual neurons: Downstream neurons could simply sum the activities of many neurons with similar sensitivities. However, because response variability is correlated across neurons (*4*, *5*), the ability of averaging to increase the signal to noise ratio is limited (*6*). Also, the fact that responses are variable does not imply that the cortex averages signals from multiple neurons, because averaging would ignore stimulus-related information encoded into which neuron fires each spike. Theoretical (*7*) and experimental (*8*, *9*) work has shown that neurons tuned to similar stimuli can convey largely independent information, especially when their responses are noisy.

Figure 1 describes two pairs of nearby V1 neurons that illustrate the range of behavior we encountered (*10*). The first pair (Fig. 1, A to D) responded robustly to the stimulus, as shown by the sharp and reliable firing rate fluctuations during typical 1-s segments (Fig. 1A). Although the neurons occasionally responded to similar stimulus features (double-headed arrow), their responses were usually distinct (single-headed arrow). Overlapping "off" subregions were evident in snapshots of the spatial receptive fields (Fig. 1B), obtained by cross-correlating the stimulus with the spike train (*10*). The "on" subregions, however, were on opposite flanks, indicating that the neurons conveyed at least some distinct spatiotemporal information. The second pair (Fig. 1, E to H) responded less robustly and more variably, and the spatial overlap was more complete.

The Pearson correlation coefficient is a measure of similarity between paired responses. We distinguished between signal correlations, which compare bin-by-bin average spike counts across trials, and noise correlations, which compare trial-by-trial deviations from the average response in each bin (*8*). The signals were essentially uncorrelated for the first pair [correlation coefficient (r) = −0.021] but highly correlated for the second (r = 0.52). The noise was uncorrelated for both pairs (r = −0.039 and −0.015, respectively).

Information rates were substantially higher for the first pair than for the second (Fig. 1, C and G) (*11*). To assess population coding, we compared two schemes: the summed-population code, which did not consider which neuron fired each spike, and the labeled-line code, which did (*12*). The summed-population information rate for the first pair was slightly higher than the information rate for the first cell alone, but the labeled-line information rate was 49% higher than the summed-population information rate. For the second pair, the difference between the summed-population and labeled-line information rates was only 5.6%. Ignoring which neuron fired each spike blurred distinctions between the responses of the first pair, resulting in a reduced multineuronal information rate. For the second pair, responses were more similar, and neuronal identity mattered less.

For each pair of neurons and code, we calculated a redundancy index as a normalized measure for comparing recording sites with vastly different information rates (*13*). The redundancy index was 0 when neurons carried independent information and 1 when the information was completely redundant. Figure 1, D and H, shows that, for both pairs, the redundancy index was higher for the summed-population code than for the labeled-line code. The difference was greater for the first pair, in which the responses were robust and distinct, so that combining spikes from those two neurons blurred distinctions and emphasized redundancy. The labeled-line code revealed the underlying independence of the responses and yielded a redundancy index of essentially 0. For the second pair, redundancy indices for both codes were near 0, meaning that the responses were almost independent, even for the summed-population code. This surprised us at first because the neurons responded to similar stimulus elements, and we gained little information when we paid attention to which neuron fired each spike. However, both signal and noise contributed to information rates, and when signals were small and correlated, and noise large and uncorrelated, information in the summed-population code was nonredundant.

We evaluated signal and noise correlations at a series of bin sizes for all pairs of neurons in our database (Fig. 2). Correlations were generally positive, but signal correlations were higher on all time scales. On short time scales, noise correlations clustered tightly about 0, whereas signal correlations were more widely distributed with positive median values <0.25. On longer time scales, median correlations reached higher levels for signal (~0.5) than for noise (~0.25). On long time scales, our results correspond approximately to other monkey visual cortex studies that used different stimuli and analyses (*3*, *8*, *14*).

Information rates and redundancy indices can be calculated for any cluster size, not just

[1]Laboratory of Biophysics, The Rockefeller University, 1230 York Avenue, New York, NY 10021, USA. [2]Department of Neurology and Neuroscience, Weill Medical College of Cornell University, 1300 York Avenue, New York, NY 10021, USA.

*To whom correspondence should be addressed. E-mail: reichd@rockefeller.edu